Sohail Reddy
Multi-Disciplinary Analysis,
Inverse Design, Robust Optimization and Controls
(MAIDROC) Lab,
Department of Mechanical and Materials
Engineering,
Florida International University,
Miami, FL 33174
e-mail:

George S. Dulikravich
Multi-Disciplinary Analysis,
Inverse Design, Robust Optimization and Controls
(MAIDROC) Lab,
Department of Mechanical and Materials
Engineering,
Florida International University,
Miami, FL 33174
e-mail:

Ann-Kayana Blanchard
Multi-Disciplinary Analysis,
Inverse Design, Robust Optimization and Controls
(MAIDROC) Lab,
Department of Mechanical and Materials
Engineering,
Florida International University,
Miami, FL 33174
e-mail:

Effects of Thin Film Heat Spreader on Hot Spots Mitigation in Heat Sinks

The effects of graphene platelets and diamond-based thin film heat spreaders on maximum temperature of integrated electronic circuits were investigated. A fully three-dimensional conjugate heat transfer analysis was performed to investigate the effects of thin film material and thickness on the temperature of a hot spot and temperature uniformity on the heated surface of the integrated circuit when subjected to forced convective cooling. Two different materials, diamond and graphene, were simulated as materials for thin films. The thin film heat spreaders were applied to the top wall of an array of micro pin fins having circular cross sections. The integrated circuit with a 4 × 3 mm footprint featured a 0.5 × 0.5 mm hot spot located on the top wall, which was also exposed to a uniform background heat flux of 500 W cm^{-2}. A hot spot uniform heat flux of magnitude 2000 W cm^{-2} was centrally situated on the top surface over a small area of 0.5 × 0.5 mm. Both isotropic and anisotropic properties of the thin film heat spreaders made of graphene platelets and diamond were computationally analyzed. The conjugate heat transfer analysis also incorporated thermal contact resistance between the thin film and the silicon substrate. It was found that isotropic thin film heat spreaders significantly reduce the hot spot temperature and increase temperature uniformity, allowing for increased thermal loads. Furthermore, it was found that thickness of the thin film heat spreader does not have to be greater than a few tens of microns. [DOI: 10.1115/1.4053168]

Keywords: thin films, heat spreaders, diamond, graphene, integrated circuit, thermal management, electronics cooling, conjugate heat transfer, forced convection, heat transfer enhancement

1 Introduction

Civilian, and especially military, applications of the new generation of micro-electronic chips are expected to reach heat flux levels of 500 W cm^{-2} at the background and in excess of 1000 W cm^{-2} at the hot spots [ ]. Soaring temperatures at these hot spots pose a major challenge to the thermal management community because they limit the processor speed. Often, forced convection cooling methods alone are not effective in lowering the temperature spikes at the hot spots. One approach to remedy this problem is to have the hot surface coated with thin film heat spreaders to lower the hot spot temperature spike and make hot surface temperature more uniform. Fukutani and Shakouri [ ] investigated Si and SiGe thin film micro-cooler and found that the hot spot temperature can be decreased by up to 30 °C. Wang et al. [ ] studied the effectiveness of thin film heat spreaders in conjunction with a micro-channel cooling configuration. Mayer and Ram [ ] performed optimization of heat sinks coated with thin films. Smalc et al. [ ] investigated the use of natural graphite as heat spreaders with much higher thermal conductivity. Reddy and Dulikravich [,] presented comparative analyses of isotropic graphene thin film and diamond thin film heat spreader performances. Graphene nano-platelets (GNPs) are a viable alternative to most thin film materials not only because they are less expensive than diamond but also because they possess a much higher directional thermal conductivity. The extremely high and anisotropic thermal conductivity makes them an ideal choice in dissipating thermal energy away from the hot spot, resulting in lower temperature and higher temperature uniformity. The effect of graphene heat spreaders on maximum temperature have been previously numerically investigated by Reddy et al. [,], Barua et al. [ ], Bae et al. [ ], and Subrina et al. [ ]. However, their work assumed that the thermal conductivity is an isotropic property, which is not always the case. The numerical methods have also ignored contact resistance between the thin films and the base substrate material.

This study investigates the effect of graphene nano-platelets and diamond thin films applied to a micro pin fin heat sink. Unlike previous computational work, these GNP thin films considered anisotropic thermal conductivity. The thermal contact resistance was also incorporated into the computational model.

2 Analysis Framework

The geometry used in this study is similar to those used in previous works [,]. An integrated circuit (IC) with a 4 × 3 mm footprint with a centrally located hotspot of size 0.5 × 0.5 mm was considered. The IC featured an array of circular cross section micro pin-fins having a diameter of 150 μm (Fig.). The height of the entire IC was 250 μm, not including the thin film. The silicon side wall thicknesses were held constant at 30 μm. Figure shows the exact dimensions, arrangement of the micro pin fins in the fluid channel and the different boundary patches of the IC + thin film configuration.

The thermal boundary conditions, hydrodynamic boundary conditions, and geometric configurations (Table) were kept constant throughout the analysis. The entire top surface was exposed to a uniform background heat flux. A significantly higher heat flux was enforced at a small, centrally located hot spot. The bottom surface, silicon sidewalls, and inlet and exit solid boundaries were thermally insulated. Water was selected as the working fluid. The outlet static (gauge) pressure was set to 20 kPa, and the inlet water temperature was 30 °C.

A computational grid of approximately 39 million cells was used for each 3D conjugate heat transfer analysis. The results obtained using a grid of 41 million grid cells showed that the

Manuscript received May 10, 2021; final manuscript received November 23, 2021; published online February 8, 2022. Assoc. Editor: Aaron P. Wemhoff.

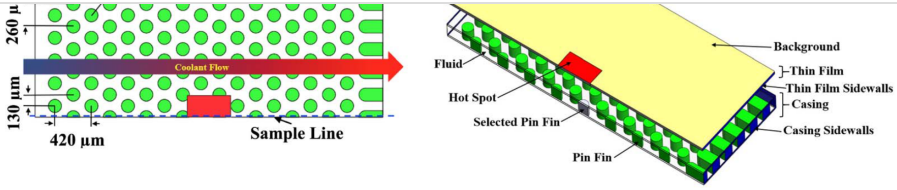

Fig. 1 One half of the integrated circuit used in this work showing: (*a*) the configuration's dimensions and (*b*) the boundary patches of the IC + thin film

results deviated by less than 1%, thereby assuring grid convergence. Five layers of clustered structured grid were placed on each solid–fluid interface. Due to symmetry, only half of the entire configuration was analyzed. The steady-state, incompressible Reynolds-averaged Navier–Stokes equations were solved for the fluid domain. The continuity, momentum, and energy equations are given as follows:

$$\nabla \cdot \mathbf{V} = 0 \tag{1}$$

$$\rho(\mathbf{V} \cdot \nabla)\mathbf{V} = \nabla \cdot \left[-p\underline{I} + \mu\left(\nabla\mathbf{V} + (\nabla\mathbf{V})^T\right)\right] \tag{2}$$

$$\rho C_p(\mathbf{V} \cdot \nabla)T = (\mathbf{V} \cdot \nabla)p + \nabla \cdot (k\nabla T) \tag{3}$$

where ρ, $\mathbf{V}$, p, T, C_p, μ, and k are the density, velocity, pressure, temperature, specific heat, viscosity, and thermal conductivity, respectively, of the fluid. The material properties were taken to be temperature independent ($\rho \neq \rho(T)$, $\mu \neq \mu(T)$, $k \neq k(T)$, and $C_p \neq C_p(T)$). The energy equation to be decoupled from the mass and momentum balance. Therefore, the mass and momentum balance equations only need to be solved once. The converged velocity and pressure fields can then be reused to solve the energy equation in the fluid domain for each thin film case.

The heat transfer in the solid region was assumed to obey Fourier's Law and be diffusive in the graphene layers since the size of the graphene layers is much larger than the phonon mean free path [13–15]. The steady-state heat conduction equation with spatially varying thermal conductivity was solved in the solid domain (thin film, pin fins, and silicon substrate).

$$\nabla \cdot (k\nabla T) = 0 \tag{4}$$

Alfieri et al. [ ] showed that even for Reynolds numbers between 80 and 180, as in this study, significant vortex shedding can still occur. For this reason, the standard $\kappa - \epsilon$ turbulence model was used to simulate the low Reynolds number flow in all cases. The numerical model defined by Eqs. – were solved using ANSYS FLUENT [ ]. Zhu et al. [ ] validated this numerical solver against experimental data obtained from cooling integrated circuits using array-jet impingement. Ghalambor et al. [ ] also validated the numerical solver against analytical solution of nonuniform, multi-stacked integrated circuits with incorporated contact resistance. Reddy et al. [ ] validated the solver against analytical solution for a case with spatially varying thermal conductivity. This shows that both the fluid domain and the solid domains are modeled accurately.

Figure shows the typical computational grid and the convergence history of each conjugate heat transfer analysis performed in this work. Since the material properties were assumed to be temperature independent, the energy equation was decoupled from the continuity, momentum balance, and turbulence model equations. This allows the previously converged velocity and pressure fields to be reused for the subsequent cases. Therefore, each subsequent case only requires the energy equation to be solved. This is seen in the spikes in temperature residuals (Fig.), where each of the eight spikes correspond to one of the eight cases (case 0–7). Each conjugate heat transfer analysis was performed using 60 cores of an Intel Xeon CPU E5-4620. It took approximately 6.5 h to analyze all eight cases of a single thickness.

The effects of thin film on temperature distribution and temperature uniformity are investigated. The uniformity is quantified using the coefficient of variation (CV) defined as follows:

$$\mathrm{CV} = \frac{\sigma}{T_{ave}} \tag{5}$$

where

$$\sigma = \sqrt{\frac{1}{N}\sum_{i=1}^{N}(T_i - T_{ave})^2} \tag{6}$$

$$T_{ave} = \frac{1}{N}\sum_{i=1}^{N} T_i \tag{7}$$

Table 1 Geometric parameters and boundary conditions used for each 3D conjugate heat analysis

Parameter	Value
IC height (μm)	250
Pin fin radius (μm)	150
Coolant inlet speed (m/s)	4
Coolant inlet temperature (K)	304
Background heat flux (W/cm^2)	500
Hot spot heat flux (W/cm^2)	2000

3 Effects of Thin Films on Integrated Circuit

This section investigates the effects of thin film thickness and thin film material on maximum temperature, temperature distribution, and temperature uniformity. Table shows the thermal conductivity of different thin film materials considered in this study.

Many works on GNP thin films in the past have neglected the effects of contact resistance. Pop et al. [ ] investigated the contact conductance of graphene on silicon dioxide. It was found that the contact resistance was on the order of 10^{-8} and ranged from 5.6×10^{-9} to 1.2×10^{-8} m^2/KW. It was slightly lower than the experimental results reported by Yu et al. [ ], indicating that contact resistance is 9×10^{-8} m^2/K W. The contact resistance for diamond–silicon interface is 3.3×10^{-8} m^2/K W [ ]. The contact

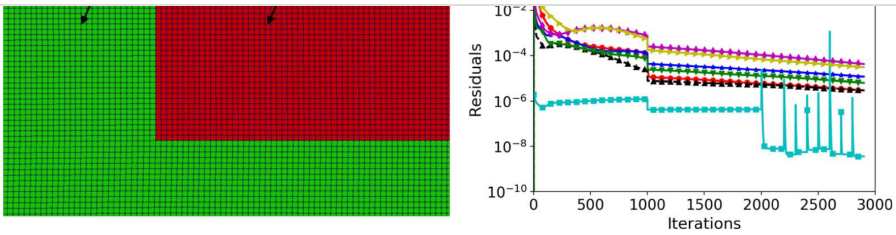

Fig. 2 Representation of a typical: (*a*) top view of a part of the thin film computational grid used and (*b*) convergence history of the conjugate heat transfer analysis performed in this work

conductance C (or contact resistance $R = 1/C$) is incorporated by modeling a thin fictitious layer of thickness Δx between the thin film and the silicon substrate [ ]. The contact resistance is defined as $R_{\text{contact}} = \Delta x / k_{\text{layer}}$, where the thermal conductivity k is appropriately selected to obtain the required resistance.

Before the results are presented, the terminology used should be discussed. This work considers the effects of thin films under two different boundary conditions.

(1) Thermally insulated thin film side walls, named the thermally insulated case
(2) Thin film side walls at a constant temperature, named the isothermal case.

All results presented in this article will be for the configuration shown in Fig. and thin film heat spreaders having thicknesses Δ of 5, 10, 15, 20, and 25 μm. For brevity, only the results of case 1, 2, 4, 6, and 7 are presented in detail.

3.1 Case 1: Isotopically Purified Graphene. For this case, the thin film material was assumed to be isotopically purified graphene, with an in-plane thermal conductivity of 4000 W/m/K and through-plane thermal conductivity of 6 W/m/K. Figure shows the temperature and normalized temperature gradients along the sample line for the cases where the thin film side walls are thermally insulated and where they are held at constant temperature. It shows that the addition of the thin film removes the oscillation in temperature and temperature gradients, thereby increasing local temperature uniformity. In the case of thermally insulated sidewalls, Figs. and , increasing thickness also increases the maximum temperature. This is due to the low thermal conductivity in the direction of greatest capability of heat removal, the water channel. Except near the hot spot, the temperature gradients are relatively small in magnitude, indicating increased temperature uniformity. The distributions due to the various thicknesses are similar, but have different mean values.

In the case where the thin film's sidewalls are held at a constant temperature, Figs. and , it can be seen that increasing thickness has little effect on the maximum temperature. Increasing the film thickness, however, does increase the background temperature. Although the top mosxt thin film layer is able to conduct heat to the sidewalls to be removed, it is unable to effectively conduct the heat to the film material underneath. These temperature distributions suggest that the profile will converge to a particular distribution with an increase in thin film thickness and that the distribution will no longer change with increasing thickness.

Figure shows the temperature distribution along the centerline of the selected pin-fin. It can be seen that an increase in film thickness leads to lower temperatures on the base of the substrate. This is because the through-plane thermal conductivity of the anisotropic film is orders of magnitude smaller than the in-plane thermal conductivity. This, combined with increasing thicknesses, restricts heat flow through to the silicon substrate. The case where the thin film's sidewalls are held at a constant temperature results in lower substrate temperatures. This is due to the additional heat that is removed through the thin film's sidewalls. For the case of thermally insulated sidewalls, it can be seen that the distribution converges with increasing thickness. The temperature at a significant number of points also increases by constant value with an increase in thickness. For the case where the film's sidewalls are held at a constant temperature, the temperature distribution again converges, but at a slower rate.

Table 2 Thermal conductivity values for each material considered [,]

Case	Material	Thermal conductivity (W/m/K) In-plane	Out-plane
0	Silicon	130	130
1	Isotopically purified graphene	4000	6
2	Isotopically mixed graphene	2000	6
3	Graphene supported by SiO_2	600	6
4	SiO_2-encased graphene	160	6
5	Bulk graphite	2000	2000
6	Natural diamond	2200	2200
7	Isotopically purified diamond	3300	3300

3.2 Case 2: Isotopically Mixed Graphene. In this section, the thin film material was assumed to be isotopically mixed graphene, with an in-plane thermal conductivity of 2000 W/m/K and an through-plane thermal conductivity of 6 W/m/K. Here, the in-plane thermal conductivity is half that of isotopically purified graphene. Figure shows the temperature along the sample line for the cases where the thin film side walls are thermally insulated and where they are held at constant temperature.

It can be seen that the distribution of temperature and temperature gradients are similar to those obtained using isotopically purified graphene. As in case 1, the temperature gradient profiles look relatively symmetric about the center point. In the case of thermally insulated thin films, for each increase of 5 μm in film thickness, the maximum temperature increases by approximately 5 K. In the case of the isothermal thin film boundary, it can be seen that the convergence to a steady-state distribution is slower than in the cases of isotopically purified graphene. In both the thermally insulated and isothermal cases, the thin films can be seen to remove temperature oscillations and improve local temperature uniformity.

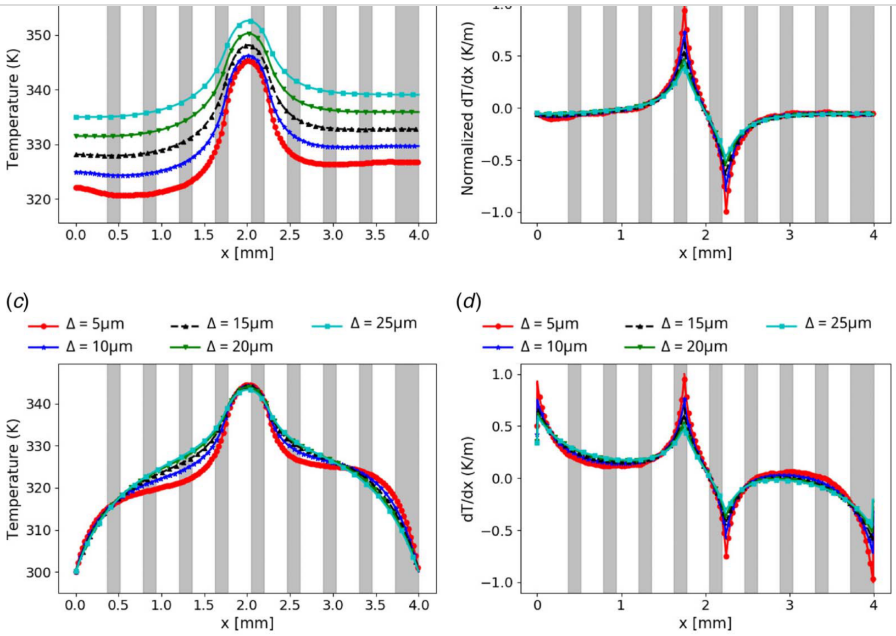

Fig. 3 Distribution along the sample line of the thin film for case 1 showing (*a*) temperature and (*b*) normalized temperature gradient for thermally insulated thin film sidewalls and (c) temperature and (*d*) normalized temperature gradient for thin film with sidewall held at constant temperature

Figure shows the temperature distribution along the centerline of the selected pin-fin. Comparing Figs. and , it can be seen that a decrease in thermal conductivity leads to a closer grouping in the temperature profiles. This suggests that the higher thermal conductivity leads to a faster convergence to the steady-state profile.

3.3 Case 4: SiO_2-Encased Graphene. In this section, the thin film was assumed to be made of SiO_2-encased graphene, with an in-plane thermal conductivity of 160 W/m/K and through-plane thermal conductivity of 6 W/m/K. Figure shows the temperature along the sample line for the cases where the thin film side walls are thermally insulated and where they are held at constant temperature.

It can be seen that in both the thermally insulated and the isothermal cases, thin films of 5 μm thickness still exhibits the local temperature oscillations. This suggests that films with lower thermal

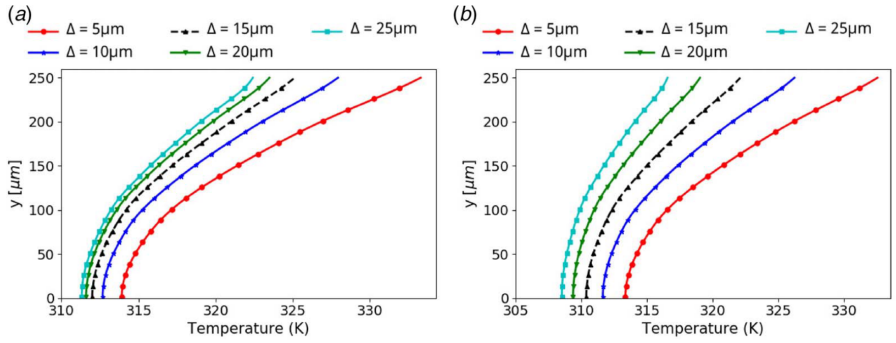

Fig. 4 Distribution along the selected pin fin's centerline for case 1 showing (*a*) temperature for thermally insulated thin film sidewalls and (*b*) temperature for thin film with sidewalls held at constant temperature

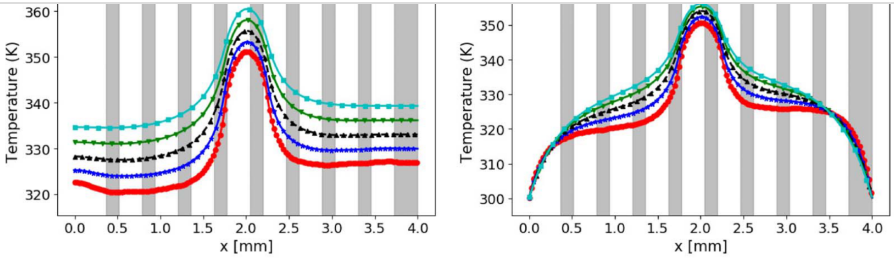

Fig. 5 Distribution along the sample line of the thin film for case 2 showing (*a*) temperature for thermally insulated thin film sidewalls and (*b*) temperature for thin film with sidewall held at constant temperature

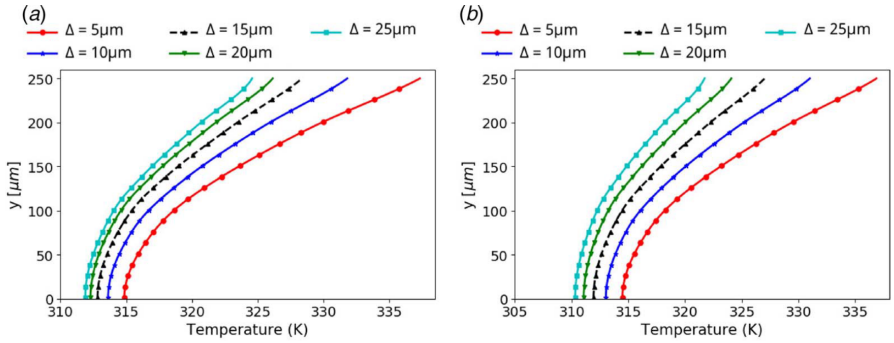

Fig. 6 Distribution along the selected pin fin's centerline for case 2 showing (*a*) temperature for thermally insulated thin film sidewalls and (*b*) temperature for thin film with sidewalls held at constant temperature

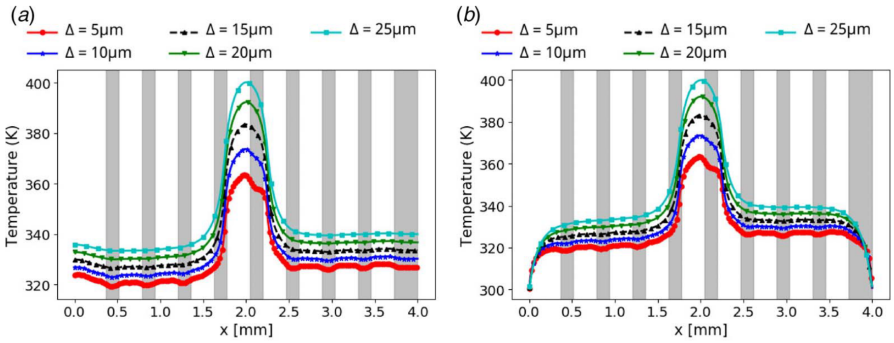

Fig. 7 Distribution along the sample line of the thin film for case 4 showing (*a*) temperature for thermally insulated thin film sidewalls and (*b*) temperature for thin film with sidewall held at constant temperature

conductivity require greater thicknesses to improve local temperature uniformity. It can be seen that thin film with thicknesses greater than 5 μm remove the temperature oscillations. The lower thermal conductivity leads to an increase in the maximum temperature and a slower convergence to the steady-state profile.

Figure shows the temperature distribution along the centerline of the selected pin fin. It shows that temperature at the base is relatively independent of the two boundary conditions applied as the thin film thermal conductivity decreases. A further decrease in thermal conductivity leads to a closer grouping of the temperature

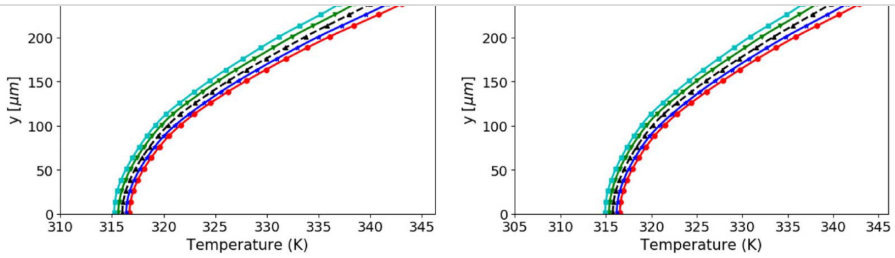

Fig. 8 Distribution along the selected pin fin's centerline for case 4 showing (*a*) temperature for thermally insulated thin film sidewalls and (*b*) temperature for thin film with sidewalls held at constant temperature

profiles. This suggests that for low conductivity films, the change in temperature with increasing thickness is much less than for the high conductivity films.

3.4 Case 6: Natural Diamond. In this section, the thin film was assumed to be made of natural diamond, with a thermal conductivity of 2200 W/m/K. Figure shows the temperature and normalized temperature gradients along the sample line for the cases where the thin film side walls are thermally insulated and where they are held at constant temperature.

Figure shows the temperature and normalized temperature gradients along the sample line for the cases when the thin film side walls are thermally insulated and held at constant temperature. It can be immediately seen that increasing the thin film thickness decreases the maximum temperature. The largest temperature decrease occurs at the hot spot for both the thermally insulated and isothermal case. It can be seen that for the thermally insulated

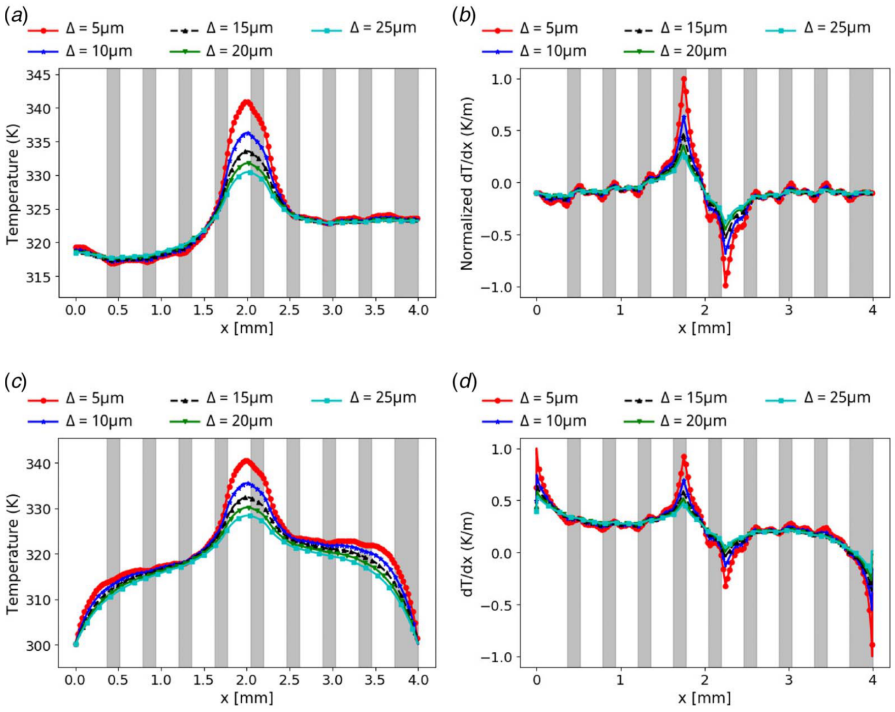

Fig. 9 Distribution along the sample line of the thin film for case 6 showing (*a*) temperature and (*b*) normalized temperature gradient for thermally insulated thin film sidewalls and (c) temperature and (*d*) normalized temperature gradient for thin film with sidewall held at constant temperature

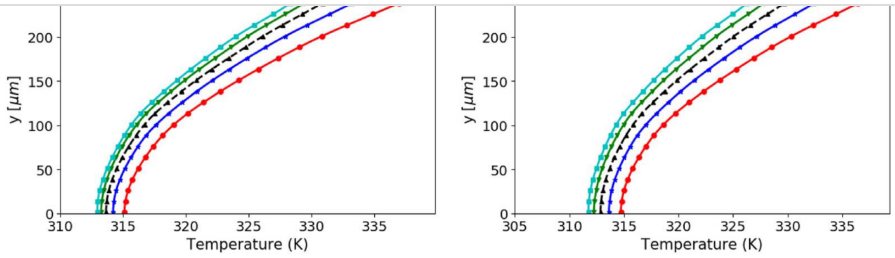

Fig. 10 Distribution along the selected pin fin's centerline for case 6 showing (*a*) temperature for thermally insulated thin film sidewalls and (*b*) temperature for thin film with sidewalls held at constant temperature

case, the temperature in the background region is relatively unchanged. This is not the case for the isothermal case, where the increasing thin film thickness also results in lower background temperatures. As in the case of anisotropic graphene thin films with low thermal conductivity, the diamond films for 5 μm do not suppress the temperature oscillations. The temperature gradients remain relatively symmetric for films of higher thicknesses. The oscillations are due to the increased conduction down into the pin fin because of the higher thermal conductivity in that direction.

Figure shows the temperature distribution along the centerline of the selected pin fin. For this case, the heat is able to be conducted away from the hot spot and into the fluid channel. It can be seen that the temperature profiles are converging with increasing film thickness. This is seen in the case of both types of boundary conditions. For greater film thicknesses, the thermally insulated thin films lead to higher temperatures than the thin films that are held at constant temperature.

3.5 Case 7: Isotopically Purified Diamond. In this section, the thin film was assumed to be made of natural diamond, with a thermal conductivity of 3000 W/m/K. Figure shows the temperature and normalized temperature gradients along the sample line for the cases where the thin film side walls are thermally insulated and held at constant temperature.

Figures and show that the change in temperature decreases with increasing film thickness. This suggests that there exists an optimal thickness after which further decrease in temperature is not possible. The same conclusion was confirmed by the excellent analytical work of Fukutani and Shakouri [ ]. For the thermally insulated case, it can be seen that the background area is relatively unaffected by the film thickness. This suggests that there is an effective area of influence beyond which the thin film heat spreader becomes ineffective. Thin films of sufficient thickness also show increased local and global temperature uniformity.

Figure shows the temperature distribution along the centerline of the selected pin fin. Again the temperature profiles for this case are similar to those of case 6. This shows a convergence in temperature with increasing thermal conductivity. Still, the higher thermal conductivity of case 7 leads to lower temperatures. It also suggests that the heat transporting capability of high thermal conductivity materials can be limited by the heat removal capability of the cooling scheme used.

3.6 Discussion and Summary. Based on the presented results, the effects of thin film (material and thickness) on the maximum temperature and CV are presented.

Figure shows the maximum temperature for thin films under the two different boundary conditions. It shows that in each anisotropic case (cases 1–4), the maximum temperature increases with thin film thickness. For thin films with a lower thermal conductivity, the increase in temperature per increase in film thickness (i.e., $\Delta T/\delta$) is larger than it is for thin films with higher thermal conductivity. The maximum temperature due to anisotropic thin films also exhibits a linear trend. The maximum temperature of isotropic thin films

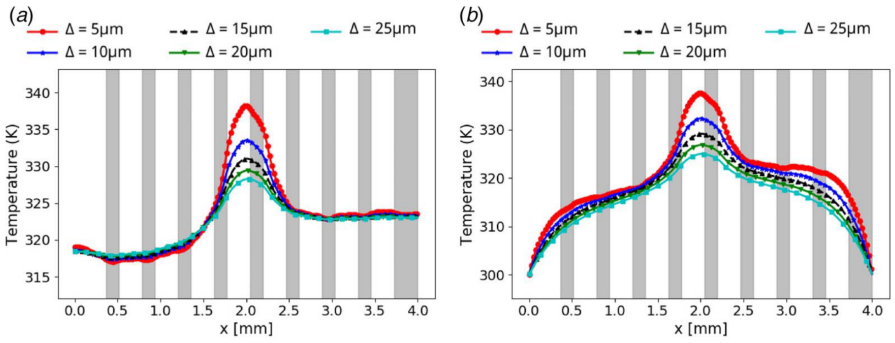

Fig. 11 Distribution along the sample line of the thin film for case 7 showing (*a*) temperature for thermally insulated thin film sidewalls and (*b*) temperature for thin film with sidewall held at constant temperature

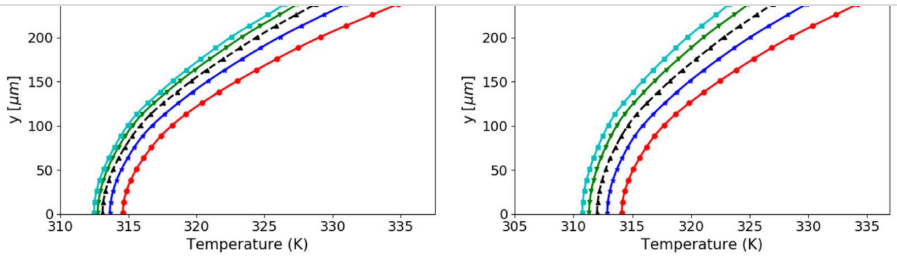

Fig. 12 Distribution along the selected pin fin's centerline for case 7 showing (*a*) temperature for thermally insulated thin film sidewalls and (*b*) temperature for thin film with sidewalls held at constant temperature

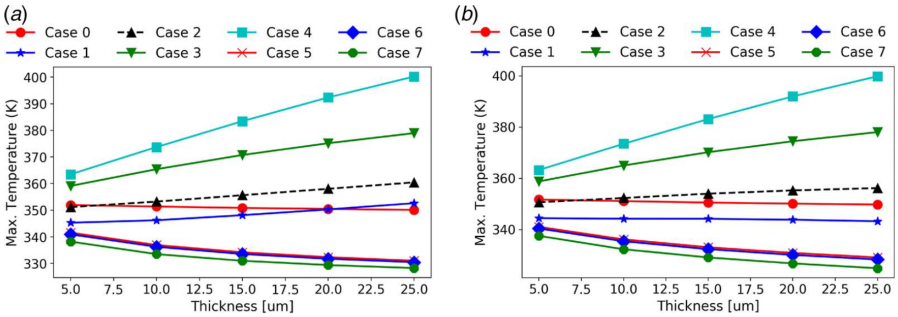

Fig. 13 The maximum temperature as a function of film thickness for (*a*) adiabatic side walls thin films and (*b*) thin films with constant temperature side walls boundary conditions

decreases with increasing thickness. The maximum temperature due to isotropic thin films exhibits a quadratically decaying trend. Similar conclusions can be drawn for the case of thin films with isothermal boundary conditions. The temperature increase on the top surface when using anisotropic films is due to their low through-plane conductivity and their inability to conduct heat into the cooling channel. The isotropic films are not only able to conduct heat laterally away from the hotspot but also down into the pin fins so that it can be removed by the working fluid.

Figure shows the temperature at the base of the selected pin fin for thin films under the two different boundary conditions. In both cases, case 1 resulted in the lowest substrate temperatures. In all cases, increasing the film thickness leads to lower substrate temperatures. A convergence in temperature with increasing thickness can also be seen. A higher thermal conductivity again leads to faster convergence. For films with lower conductivity, the change in temperature due to change in thickness is much less than for the high conductivity films. The trends in the substrate temperature

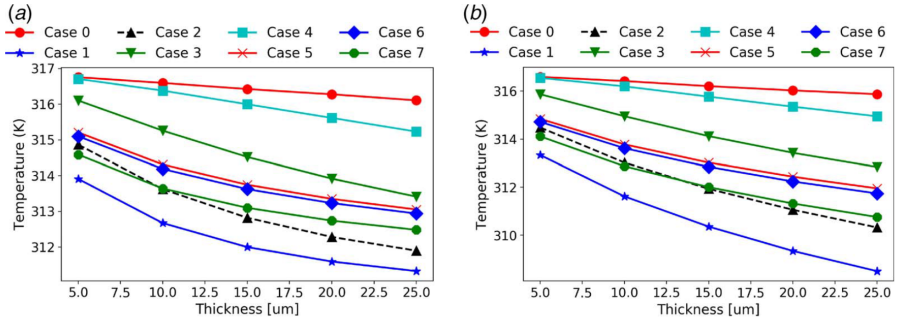

Fig. 14 The temperature at the base of the selected pin fin as a function of thin film thickness for (*a*) thermally insulated side walls films and (*b*) constant temperature side walls

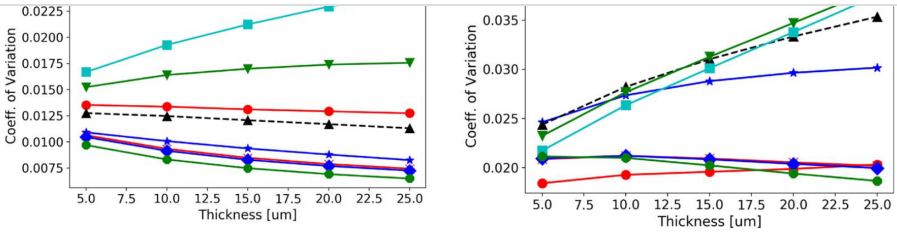

Fig. 15 The coefficient of variation (Eq.) as a function of thin film thickness for (*a*) thermally insulated side walls and (*b*) constant temperature side walls

are same for both boundary conditions. The lower substrate temperature when using anisotropic films is due to the low through-plane thermal conductivity, which restricts heat flow down to the substrate. In the case of isotropic thin films, the heat that is conducted into the substrate is removed by the working fluid, thereby leading to lower substrate temperature.

It is important to mention that thermal stresses should also be considered when investigating the applicability of thin films. In the case of the anisotropic thin films in case 1 (Figs. and), the temperature on the top surface of the substrate, with a thin film of thickness 25 μm, is approximately 320 K, whereas the maximum temperature on the top surface of the thin film is approximately 350 K. This temperature difference leads to large thermal gradients and thermal stresses. Therefore, the thermal stresses should also be considered.

Figure shows the coefficient of variation (Eq.) for thin films under the two different boundary conditions. For anisotropic thin films with lower thermal conductivity, the increase in film thickness leads to an increase in coefficient of variation and a decrease in temperature uniformity. For case 1 and 2, however, increasing film thickness leads to a reduction in coefficient of variation. This suggests that there is a critical value of thermal conductivity, after which the temperature uniformity deteriorates with increasing film thickness. For isotropic thin films, the increasing film thickness leads to increase in temperature uniformity. Thus trends in coefficient of variation for isotropic thin films are similar to those of maximum temperature.

For the case of isothermal thin films, all anisotropic films lead to an increase in coefficient of variation with increased film thickness. The isotropic thin films, however, result in a lower coefficients of variation with increasing film thickness. Figure shows that the coefficient of variation for isotropic films of smaller thickness are nearly indistinguishable.

4 Conclusion

The effects of graphene nano-platelets and diamond-based thin films as heat spreaders on a hot surface of an integrated circuit having a hot spot have been investigated. The work considered the effects of isotropic and anisotropic thermal conductivity, and thickness of thin films on maximum temperature and temperature uniformity. The effects of different boundary conditions at the thin film's sidewalls and the film/substrate contact were also investigated.

The anisotropic thin films were able to improve local temperature uniformity but were not able to lower the maximum temperature. Thin anisotropic films with high thermal conductivity were also able to improve global surface temperature uniformity, while those with low thermal conductivity adversely affected the temperature uniformity. Thickness increase of the anisotropic thin film lead to a higher maximum temperature and larger coefficient of variation of temperature. However, the anisotropic thin films did result in lower substrate temperatures.

The isotropic thin films of appropriate thickness were shown to significantly lower maximum temperature and increase both local and global surface temperature uniformity. This was demonstrated in the case of both diamond and graphene thin films. For anisotropic and isotropic films, it was confirmed that an optimum film thickness exists, beyond which the decrease in temperature is negligible. It was found that even a thin film of very small thickness can greatly reduce maximum temperature and increase temperature uniformity.

With increasing thickness, the temperature distribution on the hot surface tends to a particular distribution. A larger thermal conductivity greatly increases the rate of convergence to this particular distribution. Anisotropic thin films can be used as an insulating layer between certain components in integrated circuits (i.e., substrates) and the heat source as they can restrict heat transfer in the out-plane direction.

Acknowledgment

The first author gratefully acknowledges the financial support from Florida International University in the form of an FIU Presidential Fellowship and FIU Dissertation Year Fellowship.

Conflict of Interest

There are no conflicts of interest.

Data Availability Statement

The authors attest that all data for this study are included in the paper. Data provided by a third party listed in Acknowledgment.

References

[1] Bar-Cohen, A., 2013, "Gen-3 Thermal Management Technology: Role of Microchannels and Nanostructures in an Embedded Cooling Paradigm," , **4**(2), p. 020907.

[2] Fukutani, K., and Shakouri, A., 2006, "Optimization of Thin Film Microcoolers for Hot Spot Removal in Packaged Integrated Circuit Chips," 22nd IEEE SEMI-THERM Symposium, Dallas, TX, Mar. 14–16, pp. 130–134.

[3] Wang, P., McCluskey, P., and Bar-Cohen, A., 2013, "Hybrid Solid- and Liquid-Cooling Solution for Isothermalization of Insulated Gate Bipolar Transistor Power Electronic Devices," , **3**(4), pp. 601–611.

[4] Mayer, P. M., and Ram, R. J., 2006, "Optimization of Heat Sink-Limited Thermoelectric Generators," , **10**(2), pp. 143–155.